

Path instabilities of air bubbles rising in clean water

Mingming Wu

Department of Physics, Occidental College, Los Angeles, CA 90041, USA

Morteza Gharib

Graduate Aeronautical Laboratories, California Institute of Technology, Pasadena, CA 91125, USA

(July 6, 2021)

Experiments are conducted to study the path and shape of single air bubbles (diameter range $0.10 - 0.20\text{cm}$) rising freely in clean water. The experimental results demonstrate that the bubble shape has a bistable state, *i. e.* the bubble chooses to be in spherical or ellipsoidal shape depending on its generation mechanism. The path of a spherical/ellipsoidal bubble is found to change from a straight path to a zigzag/spiral path via a supercritical/subcritical bifurcation when the Reynolds number of the bubble exceeds a threshold.

PACS numbers: 47.27.Vf, 47.55.Dz, 47.20.Ft, 47.20.-k

The spiral or zigzag motion of air bubbles rising freely in a fluid medium have been observed in various experiments. [1–5] Extensive work has been done to determine the criteria for the onset of path instability. [3,4,6,7] Simple as the matter appears to be, it turns out that the path of the bubble itself is very sensitive to the experimental setup near the instability point, especially to the turbulence level in the fluid medium due to the background noise and the contaminations of the fluids. As a consequence, no consistent stability criteria can be found in the current literature. The exact nature of the path instability is yet to be explored.

The focus of our investigations is on the understanding of the underlying mechanism of the path instability. Recent work by Kelley and Wu [9] on path instabilities of a penny-shaped bubble rising in a Hele-Shaw cell (2-dimensional case) demonstrated that the path of a bubble was changed from a straight path to a zigzag path when the Reynolds number exceeded a critical value. Colored dye visualization experiments showed that such instability was a consequence of vortex shedding in the wake of the bubble, a reminiscence of vortex shedding in the wake of a solid cylinder. In the 3-dimensional case where bubbles rise freely in fluids, some intriguing work has been done by Lunde and Perkins [5] where the wake structures of the bubbles rising in tap water were studied using colored dye visualization technique in the Reynolds number range of 600-1700. The experimental results demonstrated a clear connection between the wake structures and the lateral motions of the bubbles.

In this letter, we present experimental investigations on the shape and path of the rising bubbles in clean water near and above the path instability point. The main part of the experimental apparatus is the plexiglass water tank with dimension $6'' \times 6'' \times 24''$. At the center of the bottom plate, a specially designed fitting is mounted for the hypodermic needle to go through. The bubble is released through the hypodermic needle. One camera is used to image the shape and size of the bubble, and

it is mounted close to the position where the bubble is released. The camera takes an image of 640×480 pixels with a viewing window of $1.25\text{cm} \times 0.936\text{cm}$. The second camera is a specially designed 3-D imaging system, [10] and it is used to map out the (x, y, z) coordinates of the bubble. The camera obtains the third dimension z (direction of rising bubble) using a quantitative defocusing mechanism. A typical viewing window of the 3-D imaging system is $1.5\text{cm} \times 1.5\text{cm} \times 20\text{cm}$. Extreme cautions were taken to keep the tank as clean as possible. Doubly deionized and distilled water was used. Large bubbles were driven through the tank for removing the surface-active contaminants prior to each experimental run. The temperature of the water tank was $24.5 \pm 0.3^\circ\text{C}$ during the experimental runs. The kinetic viscosity $\nu = 0.00901\text{ cm}^2/\text{s}$ and surface tension $\sigma = 72.1\text{ dyn/cm}$ are given by Ref. [12].

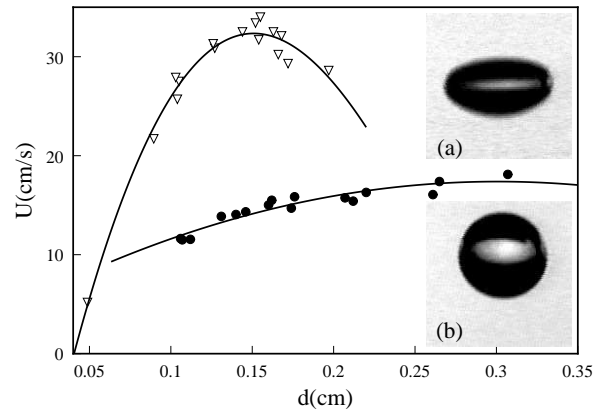


FIG. 1. Terminal velocity U versus diameter d of ∇ : ellipsoidal bubbles and \bullet : nearly spherical bubbles. Inset (a) is an image of an ellipsoidal bubble with $d = 0.172\text{cm}$, inset (b) is an image of a nearly spherical bubble with $d = 0.174\text{cm}$.

Two different bubble generation methods have been used. The first one is to attach the hypodermic needle

arXiv:patt-sol/9804002v1 7 Apr 1998

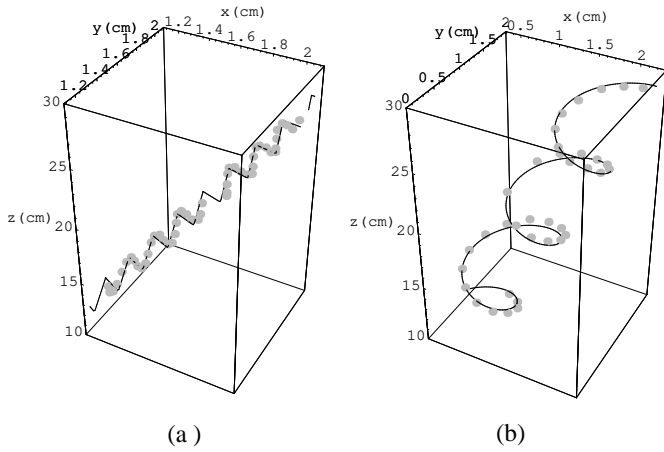


FIG. 2. (a) Zigzag path of a nearly spherical bubble at $Re = 269$. Solid line is a fit to a zigzag function. (b) Spiral path of an ellipsoidal bubble at $Re = 640$. Solid line is a fit to a spiral function. In both (a) and (b), the dotted lines are from experiments.

directly to a syringe filled with air. Push the syringe gently until a bubble is formed at the tip of the needle and then is pinched off from the needle. The size of the bubble depends on the the inner diameter of the needle and the shape of the needle tip. Using this pinch off method, we have consistently generated bubbles with ellipsoidal shape. The aspect ratios (long axis versus short axis) of the bubbles are between 1.12–1.89 for bubbles of diameter range of $0.10\text{cm} - 0.20\text{cm}$. The diameter here is defined as $(6V/\pi)^{1/3}$, where V is the volume of the bubble. V is obtained using the image taken by the CCD camera. Fig. 1 shows a typical image of an ellipsoidal bubble. For the second bubble generation method, the hypodermic needle is attached to a three way valve, of which one way is connected to a syringe filled with water and the other to a syringe pump filled with air. The hypodermic needle has a specially designed capillary tube with a flat top. The inner diameter of the tube is 0.121cm and the length of the tube is $3''$. To generate a bubble, a desired volume of air is pushed into the lower end of the capillary tube by the syringe pump, and then the direction of a three way valve is switched so that the bubble can be gently pushed out of the capillary tube by the syringe filled with water. Using this gentle push method, we were able to obtain consistently bubbles of nearly spherical shape. The aspect ratios are between 1.00 -1.07 for bubbles in the diameter range of $0.10 - 0.20\text{cm}$. A typical spherical bubble image is shown in Fig. 1. It needs to be noted here that the diameter range in which the bubble has a bistable shape state extends beyond $0.10 - 0.20\text{cm}$.

The velocities of the bubbles of various diameters are shown in Fig. 1. It demonstrates that for the same diameter, the ellipsoidal bubble moves much faster than the spherical bubble. The measured velocities of the ellip-

soidal bubbles are consistent with those obtained by

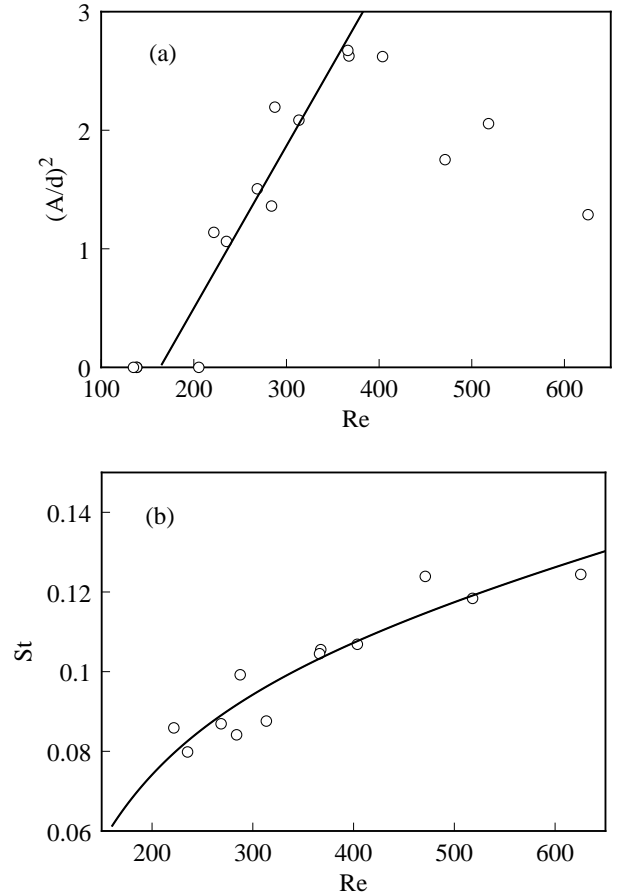


FIG. 3. (a) Curves of dimensionless amplitude squared versus Reynolds number for nearly spherical bubbles. Solid line is a fit to a linear function. (b) Curves of Strouhal versus Reynolds number. Solid line is a fit to $A/R + B + CR$, $A = -8.50, B = 0.105, C = 5.94 \times 10^{-5}$. Dotted lines are from experiments.

Maxworthy *et. al* using clean water. [8] Note that pinch off method was used in their experiment. [11]

For nearly spherical bubble, the straight path of the bubble is changed to a zigzag path as the Reynolds number Re exceeds a critical value Rec . Here Reynolds number Re is defined as Ud/ν , where U is the bubble velocity, d is the bubble diameter, and ν is the kinetic viscosity of the fluid. Typical planar zigzag path of the bubble is shown in Fig. (2a). A zigzag function is used to fit the zigzag path, and the amplitude A and the frequency f of the zigzag path is obtained from the fitted parameters. In Fig. (3a), the dimensionless amplitude squared of the zigzag path is plotted as a function of Reynolds number. As seen that the amplitude squared is linearly related to the Reynolds number near the onset of the path instability, a signature of supercritical bifurcation. The linear extrapolation of the line gives the critical Reynolds number of $Rec = 157 \pm 10$. The Strouhal curve of the zigzag path is shown in Fig. (3b). The Strouhal number here is

defined as $St = fd/U$. Colored dye visualization experi-

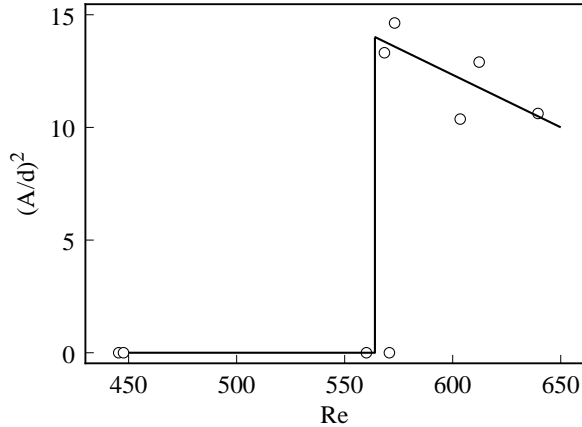


FIG. 4. Curves of dimensionless amplitude squared versus Reynolds number for ellipsoidal bubbles. Solid lines are guidelines.

ments were carried out and the results were consistent with those of Lunde and Perkins [5], where hairpin vortices were observed to shed periodically from the alternate rear sides of the zigzag bubble. This indicates that the zigzag path instability is caused by vortex shedding in the wake of the bubble, in a similar way as in the 2-D situation. [9]

The path instabilities of the ellipsoidal bubble differs from those of spherical bubble qualitatively. The straight path of the ellipsoidal bubble changes to a spiral path as shown in Fig. 2b when the Reynolds number exceeds a critical value. The measured spiral path is fitted to a spiral function, where the amplitude A and frequency of the spiral path are obtained from the fitted parameters. The curve of dimensionless amplitude squared versus Reynolds number (Fig. 4) shows that the spiral path instability occurs at $Re_c = 564 \pm 10$ via a subcritical bifurcation. The Strouhal number at the onset is ~ 0.02 . Colored dye visualization experiments on the wake structures behind spiralling bubbles by Lunde and Perskin [5] revealed two continuous vortex filaments. At present, the exact cause for the spiral instability is yet to be explored. We do notice that the short axis of the ellipsoidal bubble is always aligned with the direction of the bubble motion, it is likely that the ellipsoidal bubble spins around its short axis as it spirals up.

In summary, We find that within a certain diameter range, the bubble shape has a bistable state, it can be either in spherical or ellipsoidal shape depending on its

generation mechanism. The spherical bubble undergoes a zigzag path instability as the Reynolds number exceeds 157 ± 10 via a supercritical bifurcation. The ellipsoidal bubble undergoes a spiral path instability as the Reynolds number exceeds 564 ± 10 via a subcritical bifurcation.

Wu would like to thank Prof. Maxworthy for an insightful discussion on the subject. Wu also would like to thank members of Gharib's group who offered generous help during her summer stay at Caltech. This work is supported by the Office of Naval Research (URI research grant N00014-92-8-1618) and the Petroleum Research Fund (ACS-PRF# 32904-GB9).

-
- [1] W. L. Haberman and R. K. Morton, "An experimental investigation of the drag and shape of air bubbles rising in various fluids," David Taylor Model Basin Report 802, 1953.
 - [2] P. G. Saffman, "On the rise of small air bubbles in water," *J. Fluid Mech.* **1**, 249 (1956).
 - [3] R. A. Hartunian and W. R. Sears, "On the instability of small gas bubbles moving uniformly in various liquids", *J. Fluid Mech.* **3**, 27 (1957).
 - [4] H. Tsuge and S. Hibino, "The onset conditions of oscillatory motion of single gas bubbles rising in various liquids," *J. Chem. Engng. Japan* **10**, 66 (1977).
 - [5] K. Lunde and R. J. Perkins, "Observations on wakes behind spheroidal bubbles and particles," Paper no. FEDSM97-3530, ASME-FED Summer Meeting, Vancouver, Canada, 1997.
 - [6] G. Ryskin, L. G. Leal, "Numerical Solution of free-boundary problems in fluid mechanics. Part 2. Buoyancy-driven motion of a gas bubble through a quiescent liquid," *J. Fluid Mech.* **148**, 19 (1984).
 - [7] D. I. Meiron, "On the stability of gas bubbles rising in an inviscid fluid," *J. Fluid Mech.* **198**, 101 (1989).
 - [8] T. Maxworthy, C. Gnann, M. Kürten and F. Durst, "Experiments on the rise of air bubbles in clean viscous liquids," *J. Fluid Mech.* **321**, 421 (1996)
 - [9] Erin Kelley and Mingming Wu, "Path instabilities of rising air bubbles in a Hele-Shaw cell," *Phys. Rev. Letts.* **29**, 1265 (1997).
 - [10] C. E. Willert and M. Gharib, "Three-dimensional particle imaging with a single camera," *Experiments in Fluids* **12**, 353 (1992).
 - [11] T. Maxworthy, Private communication, 1998.
 - [12] R. C. Weast, "CRC handbook of chemistry and physics," 64th ed. (CRC press, West Palm Beach, Florida, 1985).

Path instabilities of air bubbles rising in clean water

Mingming Wu

Department of Physics, Occidental College, Los Angeles, CA 90041, USA

Morteza Gharib

Graduate Aeronautical Laboratories, California Institute of Technology, Pasadena, CA 91125, USA

(April 4, 1998)

Experiments are conducted to study the path and shape of single air bubbles (diameter range $0.10 - 0.20\text{cm}$) rising freely in clean water. The experimental results demonstrate that the bubble shape has a bistable state, *i. e.* the bubble chooses to be in spherical or ellipsoidal shape depending on its generation mechanism. The path of a spherical/ellipsoidal bubble is found to change from a straight path to a zigzag/spiral path via a supercritical/subcritical bifurcation when the Reynolds number of the bubble exceeds a threshold.

PACS numbers: 47.27.Vf, 47.55.Dz, 47.20.Ft, 47.20.-k

The spiral or zigzag motion of air bubbles rising freely in a fluid medium have been observed in various experiments. [1–5] Extensive work has been done to determine the criteria for the onset of path instability. [3,4,6,7] Simple as the matter appears to be, it turns out that the path of the bubble itself is very sensitive to the experimental setup near the instability point, especially to the turbulence level in the fluid medium due to the background noise and the contaminations of the fluids. As a consequence, no consistent stability criteria can be found in the current literature. The exact nature of the path instability is yet to be explored.

The focus of our investigations is on the understanding of the underlying mechanism of the path instability. Recent work by Kelley and Wu [9] on path instabilities of a penny-shaped bubble rising in a Hele-Shaw cell (2-dimensional case) demonstrated that the path of a bubble was changed from a straight path to a zigzag path when the Reynolds number exceeded a critical value. Colored dye visualization experiments showed that such instability was a consequence of vortex shedding in the wake of the bubble, a reminiscence of vortex shedding in the wake of a solid cylinder. In the 3-dimensional case where bubbles rise freely in fluids, some intriguing work has been done by Lunde and Perkins [5] where the wake structures of the bubbles rising in tap water were studied using colored dye visualization technique in the Reynolds number range of 600–1700. The experimental results demonstrated a clear connection between the wake structures and the lateral motions of the bubbles.

In this letter, we present experimental investigations on the shape and path of the rising bubbles in clean water near and above the path instability point. The main part of the experimental apparatus is the plexiglass water tank with dimension $6'' \times 6'' \times 24''$. At the center of the bottom plate, a specially designed fitting is mounted for the hypodermic needle to go through. The bubble is released through the hypodermic needle. One camera is used to image the shape and size of the bubble, and

it is mounted close to the position where the bubble is released. The camera takes an image of 640×480 pixels with a viewing window of $1.25\text{cm} \times 0.936\text{cm}$. The second camera is a specially designed 3-D imaging system, [10] and it is used to map out the (x, y, z) coordinates of the bubble. The camera obtains the third dimension z (direction of rising bubble) using a quantitative defocusing mechanism. A typical viewing window of the 3-D imaging system is $1.5\text{cm} \times 1.5\text{cm} \times 20\text{cm}$. Extreme cautions were taken to keep the tank as clean as possible. Doubly deionized and distilled water was used. Large bubbles were driven through the tank for removing the surface-active contaminants prior to each experimental run. The temperature of the water tank was $24.5 \pm 0.3^\circ\text{C}$ during the experimental runs. The kinetic viscosity $\nu = 0.00901\text{cm}^2/\text{s}$ and surface tension $\sigma = 72.1\text{dyn}/\text{cm}$ are given by Ref. [12].

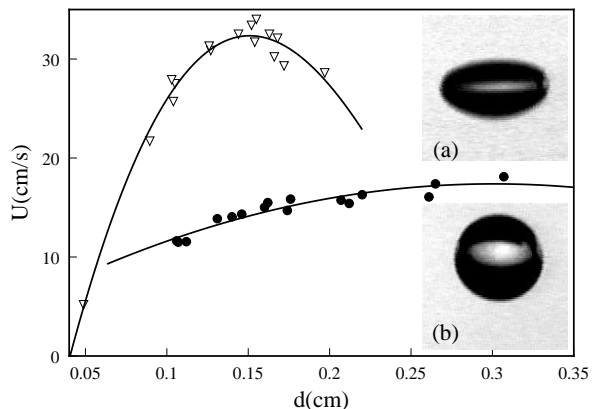


FIG. 1. Terminal velocity U versus diameter d of ∇ : ellipsoidal bubbles and \bullet : nearly spherical bubbles. Inset (a) is an image of an ellipsoidal bubble with $d = 0.172\text{cm}$, inset (b) is an image of a nearly spherical bubble with $d = 0.174\text{cm}$.

Two different bubble generation methods have been used. The first one is to attach the hypodermic needle

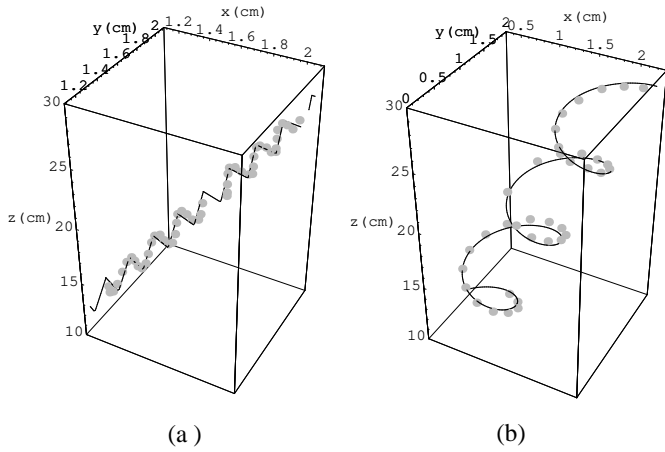


FIG. 2. (a) Zigzag path of a nearly spherical bubble at $Re = 269$. Solid line is a fit to a zigzag function. (b) Spiral path of an ellipsoidal bubble at $Re = 640$. Solid line is a fit to a spiral function. In both (a) and (b), the dotted lines are from experiments.

directly to a syringe filled with air. Push the syringe gently until a bubble is formed at the tip of the needle and then is pinched off from the needle. The size of the bubble depends on the the inner diameter of the needle and the shape of the needle tip. Using this pinch off method, we have consistently generated bubbles with ellipsoidal shape. The aspect ratios (long axis versus short axis) of the bubbles are between 1.12–1.89 for bubbles of diameter range of $0.10\text{cm} - 0.20\text{cm}$. The diameter here is defined as $(6V/\pi)^{1/3}$, where V is the volume of the bubble. V is obtained using the image taken by the CCD camera. Fig. 1 shows a typical image of an ellipsoidal bubble. For the second bubble generation method, the hypodermic needle is attached to a three way valve, of which one way is connected to a syringe filled with water and the other to a syringe pump filled with air. The hypodermic needle has a specially designed capillary tube with a flat top. The inner diameter of the tube is 0.121cm and the length of the tube is $3''$. To generate a bubble, a desired volume of air is pushed into the lower end of the capillary tube by the syringe pump, and then the direction of a three way valve is switched so that the bubble can be gently pushed out of the capillary tube by the syringe filled with water. Using this gentle push method, we were able to obtain consistently bubbles of nearly spherical shape. The aspect ratios are between 1.00 -1.07 for bubbles in the diameter range of $0.10 - 0.20\text{cm}$. A typical spherical bubble image is shown in Fig. 1. It needs to be noted here that the diameter range in which the bubble has a bistable shape state extends beyond $0.10 - 0.20\text{cm}$.

The velocities of the bubbles of various diameters are shown in Fig. 1. It demonstrates that for the same diameter, the ellipsoidal bubble moves much faster than the spherical bubble. The measured velocities of the ellip-

soidal bubbles are consistent with those obtained by

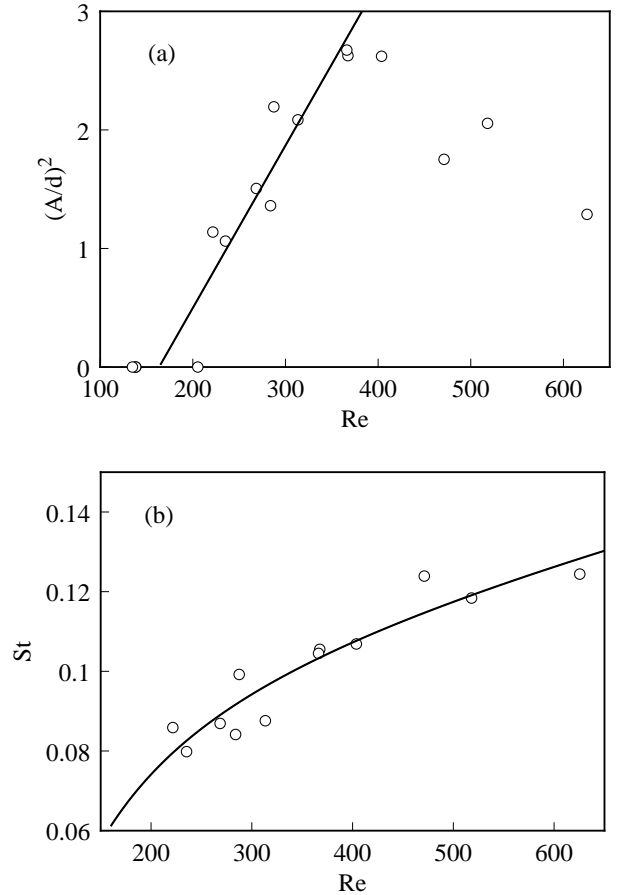


FIG. 3. (a) Curves of dimensionless amplitude squared versus Reynolds number for nearly spherical bubbles. Solid line is a fit to a linear function. (b) Curves of Strouhal versus Reynolds number. Solid line is a fit to $A/R + B + CR$, $A = -8.50, B = 0.105, C = 5.94 \times 10^{-5}$. Dotted lines are from experiments.

Maxworthy *et. al* using clean water. [8] Note that pinch off method was used in their experiment. [11]

For nearly spherical bubble, the straight path of the bubble is changed to a zigzag path as the Reynolds number Re exceeds a critical value Rec . Here Reynolds number Re is defined as Ud/ν , where U is the bubble velocity, d is the bubble diameter, and ν is the kinetic viscosity of the fluid. Typical planar zigzag path of the bubble is shown in Fig. (2a). A zigzag function is used to fit the zigzag path, and the amplitude A and the frequency f of the zigzag path is obtained from the fitted parameters. In Fig. (3a), the dimensionless amplitude squared of the zigzag path is plotted as a function of Reynolds number. As seen that the amplitude squared is linearly related to the Reynolds number near the onset of the path instability, a signature of supercritical bifurcation. The linear extrapolation of the line gives the critical Reynolds number of $Rec = 157 \pm 10$. The Strouhal curve of the zigzag path is shown in Fig. (3b). The Strouhal number here is

defined as $St = fd/U$. Colored dye visualization experi-

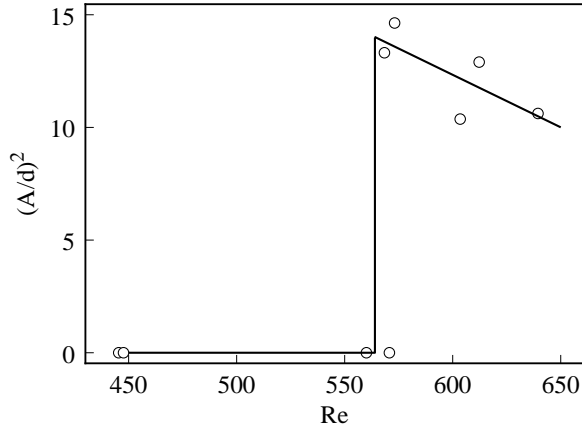


FIG. 4. Curves of dimensionless amplitude squared versus Reynolds number for ellipsoidal bubbles. Solid lines are guidelines.

ments were carried out and the results were consistent with those of Lunde and Perkins [5], where hairpin vortices were observed to shed periodically from the alternate rear sides of the zigzag bubble. This indicates that the zigzag path instability is caused by vortex shedding in the wake of the bubble, in a similar way as in the 2-D situation. [9]

The path instabilities of the ellipsoidal bubble differs from those of spherical bubble qualitatively. The straight path of the ellipsoidal bubble changes to a spiral path as shown in Fig. 2b when the Reynolds number exceeds a critical value. The measured spiral path is fitted to a spiral function, where the amplitude A and frequency of the spiral path are obtained from the fitted parameters. The curve of dimensionless amplitude squared versus Reynolds number (Fig. 4) shows that the spiral path instability occurs at $Re_c = 564 \pm 10$ via a subcritical bifurcation. The Strouhal number at the onset is ~ 0.02 . Colored dye visualization experiments on the wake structures behind spiralling bubbles by Lunde and Perskin [5] revealed two continuous vortex filaments. At present, the exact cause for the spiral instability is yet to be explored. We do notice that the short axis of the ellipsoidal bubble is always aligned with the direction of the bubble motion, it is likely that the ellipsoidal bubble spins around its short axis as it spirals up.

In summary, We find that within a certain diameter range, the bubble shape has a bistable state, it can be either in spherical or ellipsoidal shape depending on its

generation mechanism. The spherical bubble undergoes a zigzag path instability as the Reynolds number exceeds 157 ± 10 via a supercritical bifurcation. The ellipsoidal bubble undergoes a spiral path instability as the Reynolds number exceeds 564 ± 10 via a subcritical bifurcation.

Wu would like to thank Prof. Maxworthy for an insightful discussion on the subject. Wu also would like to thank members of Gharib's group who offered generous help during her summer stay at Caltech. This work is supported by the Office of Naval Research (URI research grant N00014-92-8-1618) and the Petroleum Research Fund (ACS-PRF# 32904-GB9).

-
- [1] W. L. Haberman and R. K. Morton, "An experimental investigation of the drag and shape of air bubbles rising in various fluids," David Taylor Model Basin Report 802, 1953.
 - [2] P. G. Saffman, "On the rise of small air bubbles in water," *J. Fluid Mech.* **1**, 249 (1956).
 - [3] R. A. Hartunian and W. R. Sears, "On the instability of small gas bubbles moving uniformly in various liquids", *J. Fluid Mech.* **3**, 27 (1957).
 - [4] H. Tsuge and S. Hibino, "The onset conditions of oscillatory motion of single gas bubbles rising in various liquids," *J. Chem. Engng. Japan* **10**, 66 (1977).
 - [5] K. Lunde and R. J. Perkins, "Observations on wakes behind spheroidal bubbles and particles," Paper no. FEDSM97-3530, ASME-FED Summer Meeting, Vancouver, Canada, 1997.
 - [6] G. Ryskin, L. G. Leal, "Numerical Solution of free-boundary problems in fluid mechanics. Part 2. Buoyancy-driven motion of a gas bubble through a quiescent liquid," *J. Fluid Mech.* **148**, 19 (1984).
 - [7] D. I. Meiron, "On the stability of gas bubbles rising in an inviscid fluid," *J. Fluid Mech.* **198**, 101 (1989).
 - [8] T. Maxworthy, C. Gnann, M. Kürten and F. Durst, "Experiments on the rise of air bubbles in clean viscous liquids," *J. Fluid Mech.* **321**, 421 (1996)
 - [9] Erin Kelley and Mingming Wu, "Path instabilities of rising air bubbles in a Hele-Shaw cell," *Phys. Rev. Letts.* **29**, 1265 (1997).
 - [10] C. E. Willert and M. Gharib, "Three-dimensional particle imaging with a single camera," *Experiments in Fluids* **12**, 353 (1992).
 - [11] T. Maxworthy, Private communication, 1998.
 - [12] R. C. Weast, "CRC handbook of chemistry and physics," 64th ed. (CRC press, West Palm Beach, Florida, 1985).